*Engineering Applications of Computational Fluid Mechanics*, 2015
http://dx.doi.org/10.1080/19942060.2015.1031318

Taylor & Francis
Taylor & Francis Group

RESEARCH ARTICLE

# Evaluating wave forces on groups of three and nine cylinders using a 3D numerical wave tank

Arun Kamath*, Mayilvahanan Alagan Chella, Hans Bihs and Øivind A. Arntsen

*Department of Civil and Transport Engineering, Norwegian University of Science and Technology, Trondheim, Norway.*

(*Received 5 November 2014; final version received 16 March 2015*)

The evaluation of the complex wave regime due to wave interaction with a large group of cylinders placed in proximity requires an efficient and accurate numerical model. This paper presents the application of a two-phase Computational Fluid Dynamics (CFD) model to carry out a detailed investigation of wave forces and flow around vertical circular cylinders placed in groups of different configurations at low Keulegan-Carpenter (KC) numbers. The 3D numerical wave tank is validated by comparing the numerical results with experimental data. Further, the hydrodynamic effects associated with three cylinders placed in tandem, side by side and in a 3 × 3 square array of nine cylinders are investigated. Wave forces are seen to reduce along the row in a tandem array. In a side-by-side arrangement, the central cylinder experiences the highest force. A combination of these effects is seen in the 3 × 3 square array. The variation of the wave forces on the cylinders in the array for different center-to-center distances and incident wavelengths is evaluated and the results show that the wave forces are the highest on the cylinders when the center-to-center distance is slightly less than half the incident wavelength.

**Keywords:** CFD; wave forces; multiple cylinders; numerical wave tank; level set method

## 1. Introduction

Cylindrical structures are commonly seen in marine environments as support structures for oil and gas platforms and offshore wind turbines. The study of wave interaction with a group of cylinders and the accurate assessment of the wave forces acting on each of the cylinders is important for design considerations. The ratio of the diameter of a single cylinder to the wavelength of the incident waves leads to different wave force regimes on the cylinder, which is determined by the Keulegan-Carpenter number $KC = UT/D$, where $U$ is the amplitude of the horizontal water particle velocity, $T$ is the wave period and $D$ is the diameter of the cylinder. When $KC > 2$, the total force on a single cylinder is calculated using the Morison formula (Morison, O'Brien, Johnson, & Schaaf, 1950) as a sum of the inertia and drag forces. The formula uses experimentally determined coefficients to calculate the total wave force on the cylinder. When $KC < 2$, the wave forces are inertia-dominated and the MacCamy-Fuchs theory (MacCamy & Fuchs, 1954) is used to determine the total wave force on a single cylinder. In this force regime, the effect of wave diffraction is important and the incident waves are scattered by the cylinder. In the case of multiple vertical cylinders in a diffraction regime, the incident waves and the diffracted waves are scattered multiple times, leading to complex wave interactions in the vicinity of the cylinders. This phenomenon of multiple scattering from the different cylinders influences the wave forces on each of the cylinders in the group. Ohkusu (1974) proposed an iterative method to evaluate the successive scattering from floating structures in a group to determine the wave force experienced by each structure. The velocity potential functions used to evaluate the successive scattering become complicated as the number of structures increases. Spring and Monkmeyer (1974) presented a method with all the boundary conditions imposed at once to obtain a matrix equation to solve the problem. Linton and Evans (1990) improved on Spring and Monkmeyer by proposing a method based on potential theory to calculate the wave forces on each of the cylinders placed in a group. This method is employed in this paper for the comparison of numerical results in the case of multiple cylinders.

Several studies have presented numerical wave tanks based on boundary integral equations (Isaacson 1982; Kim, Liu, & Ligget, 1983; Longuet-Higgins & Cokelet, 1976) and Boussinesq equations (Nwogu, 1993; Wei & Kirby, 1995). The numerical wave tanks based on boundary integral equations are limited in their application due to being single phase and due to the assumption of the irrotational flow. Boussinesq equations are depth-averaged, two-dimensional and valid only in intermediate and shallow waters. The Navier-Stokes equations include three-dimensional flow features, the effects of rotational flow, viscosity and higher order non-linear wave

*Corresponding author. Email: arun.kamath@ntnu.no

interactions between the cylinders. Computational Fluid Dynamics (CFD) simulations provide a great amount of detail concerning the free surface around obstacles in the flow, the pressure and forces acting on an object, and the velocity of fluid particles. With an accurate representation of the free surface, the various flow features can be studied, including wave diffraction and the evolution of the diffracted and reflected waves and their influence on the wave forces experienced by the objects. In the current literature, CFD methods have been used to investigate wave propagation in coastal regions (Jacobsen, Fuhrman, & Fredsøe, 2011; Morgan et al., 2010), wave interaction with coastal structures (del Jesus et al., 2012; Higuera, Lara, & Losada, 2014) and modeling of breaking waves (Alagan Chella, Bihs, Myrhaug, & Muskulus, 2015). Two-phase models are essential for obtaining a good representation of free surface flows due to the interaction of air and water at the interface (Liu & Yang, 2014). Numerical methods such as Smoothed Particle Hydrodynamics (SPH) have also been used to model the interaction of fluids with structures (Pu, Shao, Huang, & Hussain, 2013). Three-dimensional numerical modeling of flow and transport over large domains can provide insights into the large-scale phenomena which can have a significant impact on the engineering solutions in the field of river, estuarine and coastal engineering and management (Chau & Jiang, 2001, 2004).

The objective of this paper is to obtain insights into the physical processes and hydrodynamic features associated with wave interaction with multiple cylinders placed in groups in different configurations using the open-source CFD model REEF3D (Alagan Chella, Bihs, Myrhaug, & Muskulus, 2015). CFD can deliver deep insight into the underlying flow physics and wave kinematics, and produce accurate and detailed results without the assumptions and simplifications of typical wave models. The evaluation of the complex wave diffraction regime in the case of multiple cylinders placed in proximity is challenging due to the multiple wave reflection and interference effects involved. The center-to-center distance between the cylinders is also an important factor influencing the wave forces, and lower-order methods using potential theory cannot account for the hydrodynamics when the cylinders are spaced very close together.

The model is validated by comparing the numerical results with data from the large-scale experiments carried out in the Large Wave Flume (GWK) in Hannover, Germany (Mo, Irschik, Oumeraci, & Liu, 2007) for the wave kinematics and the wave forces on a single cylinder. Further, numerical simulations are carried out with three cylinders in tandem and three cylinders placed side by side. The final case is a combination of the two arrangements, with nine cylinders placed in a 3 × 3 square array. The effect of the center-to-center distance and the incident wavelength on the wave forces experienced by each of the cylinders in the array is studied.

## 2. Numerical model: REEF3D

The incompressible Reynolds-Averaged Navier-Stokes (RANS) equations are used to solve the fluid flow problem:

$$\frac{\partial U_i}{\partial x_i} = 0 \tag{1}$$

$$\frac{\partial U_i}{\partial t} + U_j \frac{\partial U_i}{\partial x_j} = -\frac{1}{\rho}\frac{\partial P}{\partial x_i} + \frac{\partial}{\partial x_j}\left[(\nu + \nu_t)\left(\frac{\partial U_i}{\partial x_j} + \frac{\partial U_j}{\partial x_i}\right)\right] + g_i \tag{2}$$

where $U_i$ is the time averaged velocity, $\rho$ is the density of water, $P$ is the pressure, $\nu$ is the kinematic viscosity, $\nu_t$ is the eddy viscosity, $t$ is time and $g$ is the acceleration due to gravity. The pressure is treated using Chorin's projection method (Chorin, 1968) and the resulting Possion pressure equation is solved using a preconditioned BiCGStab solver (van der Vorst, 1992). Turbulence modeling is carried out using the two-equation $k-\omega$ model proposed by Wilcox (1994). Eddy viscosity, $\nu_t$, is bounded to avoid unphysical overproduction of turbulence in strained flow by using a stress limiter in the definition of eddy viscosity (Bradshaw, Ferriss, & Atwell, 1967) as shown by Durbin (2009). The large difference in density of air and water in a two-phase model leads to an overproduction of turbulence at the interface due to the large strain. Free surface turbulence damping using a limiter around the interface for the source terms as shown by Naot and Rodi (1982) is carried out to avoid the unphysical overproduction of turbulence at the interface. The damping is carried out only around the interface using the smoothed Dirac delta function.

The fifth-order conservative finite difference Weighted Essentially Non-Oscillatory (WENO) scheme proposed by Jiang and Shu (1996) is used for the discretization of convective terms for the velocity $U_i$, the level set function $\phi$, the turbulent kinetic energy $k$ and the specific turbulent dissipation rate $\omega$. A Total Variation Diminishing (TVD) third-order Runge-Kutta explicit time scheme developed by Harten (1983) is employed for time discretization in the model. This is a three-step scheme and involves the calculation of the spatial derivatives three times per time step. This scheme is used for the time advancement of the level set function and the re-initialization equation. An adaptive time stepping approach is used to maintain the time step in accordance with the Courant-Friedrichs-Lewy (CFL) criterion for numerical stability (Griebel, Dornsheifer, & Neunhoeffer, 1998).

The free surface is obtained using the level set method where the zero level set of a signed distance function, $\phi(\vec{x}, t)$ is used to represent the interface between air and water (Osher & Senthian, 1988). Moving away from the interface, the level set function gives the closest distance of the point from the interface. The sign of the function represents the two fluids across the interface, as shown in

Equation (3):

$$\phi(\vec{x},t)\begin{cases} > 0 & \text{if} \quad \vec{x} \text{ is in air} \\ = 0 & \text{if} \quad \vec{x} \text{ is at the interface} \\ < 0 & \text{if} \quad \vec{x} \text{ is in water} \end{cases} \tag{3}$$

The velocity field in the simulation moves the level set function using the convection equation:

$$\frac{\partial \phi}{\partial t} + U_j \frac{\partial \phi}{\partial x_j} = 0 \tag{4}$$

The level set method is re-initialized after every iteration using a partial differential equation (PDE) based re-initialization procedure presented by Sussman et al. (1994):

$$\frac{\partial \phi}{\partial t} + S(\phi)\left(\left|\frac{\partial \phi}{\partial x_j}\right| - 1\right) = 0 \tag{5}$$

where $S(\phi)$ is the smoothed sign function by Peng, Merriman, Osher, Zhao, and Kang (1999) to retain its signed distance property after convection:

$$S(\phi) = \frac{\phi}{\sqrt{\phi^2 + \left|\frac{\partial \phi}{\partial x_j}\right|^2 (\Delta x)^2}} \tag{6}$$

The jump in density and viscosity at the interface is handled with the regularized Heaviside function over a thickness of $2.1\Delta x$ around the interface.

A uniform Cartesian grid is used in the numerical model for spatial discretization. The Immersed Boundary Method (IBM; Peskin, 1972) is used to incorporate the boundary conditions for complex geometries. In the current study, a local directional ghost cell IBM presented by Berthelsen and Faltinsen (2008) is implemented using object-oriented programming techniques, where the ghost cell values can be updated from multiple directions (Bihs, 2011). The ghost cells store multiple values and return a particular value when called from the respective direction.

The relaxation method (Mayer, Garapon, & Sørensen, 1998) is used for wave generation and absorption in the numerical wave tank. This method uses a wave generation zone and a wave absorption zone to moderate the computational values and the analytical values given by wave theory. The relaxation function proposed by Jacobsen et al. (2012) presented in Equation (7) is used in this study:

$$\Gamma(x) = 1 - \frac{\exp(x^{3.5}) - 1}{\exp(1) - 1} \text{ for } x \in [0;1] \tag{7}$$

where $x$ is the coordinate along the $x$-axis scaled to the length of the relaxation zone. In the wave generation zone, the values for the free surface elevation and the velocity given by wave theory are prescribed to the computational values using the relaxation function $\Gamma(x)$, as shown in Equation (8), and the generated waves are released into the working zone of the wave tank. In the wave absorption zone, the relaxation function is operated as $\Gamma(1-x)$. The computational values of velocity and free surface from the working zone are reduced to zero and the wave energy is smoothly removed from the computational domain.

$$\begin{aligned} U_{\text{relaxed}} &= \Gamma(x)\, U_{\text{analytical}} + (1 - \Gamma(x))\, U_{\text{computational}} \\ \phi_{\text{relaxed}} &= \Gamma(x)\, \phi_{\text{analytical}} + (1 - \Gamma(x))\, \phi_{\text{computational}} \end{aligned} \tag{8}$$

The free surface, horizontal and vertical water particle velocities for linear wave theory are given by Equations (9), (10) and (11) respectively:

$$\eta = A\, \sin(\omega t - \kappa x) \tag{9}$$

$$u = \omega A \frac{\cosh \kappa(z+d)}{\sinh \kappa d} \sin(\omega t - \kappa x) \tag{10}$$

$$w = \omega A \frac{\sinh \kappa(z+d)}{\sinh \kappa d} \cos(\omega t - \kappa x) \tag{11}$$

where $A$ is the wave amplitude, $\kappa$ is the wave number $= 2\pi/L$, $L$ is the wavelength, $\omega$ is the angular wave frequency and $d$ is the water depth. Typically, the wave generation zone is one wavelength long and the absorption zone is two wavelengths long. The computational efficiency of the program is increased by parallelizing the code using a Message Passing Interface (MPI). Here the domain is decomposed into smaller pieces and each assigned to a processor. So the program runs separately on each processor and the values between the processes are communicated using the MPI library.

## 3. Calculation of wave forces

### 3.1. *Calculation of wave forces in the numerical model*

The wave force on an object is calculated as the integral of the pressure and the shear stress around the surface of the object as follows:

$$F = \int_{\Omega} (-\vec{n}\mathrm{P} + \vec{n} \cdot \tau)\, d\Omega \tag{12}$$

where $\vec{n}$ and $\tau$ are a unit normal vector and a viscous stress tensor, respectively. This is easily accomplished in the numerical model as the values for the pressure at every point in the domain are available from the solution of the Poisson pressure equation. No-slip boundary conditions are imposed on the boundary between the object and the fluid domain.

### 3.2. *Analytical formula for calculating wave forces on multiple cylinders*

Wave forces on cylinders in an inertia-dominated force regime ($KC < 2$) can be calculated using the MacCamy-Fuchs formula (MacCamy & Fuchs, 1954), which is based

on potential theory:

$$F_0 = \left| \frac{4\rho g i A \tanh(\kappa d)}{\kappa^2 H_1'(\kappa a)} \right| \tag{13}$$

where $F_0$ is the inline force on a single cylinder, $i = \sqrt{-1}$, $d$ is the water depth, $a$ is the radius of the cylinder and $H_1'$ is the derivative of the Hankel function of the first kind.

Linton and Evans (1990) presented a theory to evaluate the wave forces experienced by each of the $N$ cylinders placed in an array by solving a system of $N(2M + 1)$ unknowns, where $M$ is order of the solution:

$$A_m^k + \sum_{j=1, j\neq k}^{N} \sum_{n=-M}^{M} A_n^j Z_n^j e^{i(n-m)\alpha_{jk}} H_{n-m}(\kappa R_{jk}) = -I_k e^{im(\pi/2-\beta)}, \; k = 1, \ldots, N, m = -M, \ldots, M. \tag{14}$$

where $A_m^k$ and $A_n^j$ are unknown coefficients of the scattered radiating wave from the $k$th and the $j$th cylinders, $Z_n^j = J_n'(\kappa a)/H_n'(\kappa a)$, where $\kappa$ is the wave number, $J'$ is the derivative of the Bessel function of the first kind, $\alpha_{jk}$ is the angle between the $x$-axis and the line connecting the centers of cylinders $j$ and $k$, $R_{jk}$ is the center-to-center distance of the cylinders $j$ and $k$, $I_k$ is the incident wave potential on cylinder $k$ and $\beta$ is the angle of wave incidence with the $x$-axis.

$$\left| \frac{F^j}{F_0} \right| = \frac{1}{2} |A_{-1}^j \pm A_1^j| \tag{15}$$

where $F^j$ is the force on the $j$th cylinder. The subtraction of the coefficients in Equation (15) gives the force on the cylinder along the $x$-axis and the addition of the coefficients gives the force along the $y$-axis.

## 4. Results and discussion

### 4.1. Validation of wave force calculation

A numerical simulation is carried out to determine the wave force on a single cylinder due to a regular wave. The wave parameters from the Large Wave Flume (GWK) experiments (Mo et al., 2007) are used in this simulation. The numerical wave tank is 132 m long, 5 m wide and 8 m high. A regular wave of height 1.2 m and wave period $T = 4.0$ s is generated in a water depth of $d = 4.76$ m. A cylinder of diameter $D = 0.7$ m is placed 44 m from the wave generation zone to provide sufficient length for the waves to propagate (Figure 1) and avoid the influence of waves reflected from the cylinder on the incident waves. The grid resolution required to represent the cylinder geometry in the domain and accurately compute the wave forces is quantified by the number of cells contained in a square with a side equal to the diameter of the cylinder. By this definition, a grid size of 0.1 m is used with a density of 49 cells/$D^2$ and 5.28 million cells in the domain. Wall boundary conditions are enforced on the side walls and bottom of the numerical domain and the symmetry plane boundary condition is applied at the top.

The free surface elevation is measured near the wall along the front line of the cylinder (WG 1), in front of the cylinder (WG 2), at the side (WG 3) and behind the cylinder (WG 4), as shown in Figure 1. The water particle velocities near the wall along the frontline of the cylinder are measured at the depths of $z = -0.93$ m, $-1.53$ m and $-2.73$ m in experiments using Acoustic Doppler Velocimeters (ADVs).

The wave forces acting on the cylinder are calculated and compared to the experimental results (Figure 2(a)) and the numerical results are seen to match the experimental observations very well. A grid refinement study is carried out for the wave forces and simulations are carried out with 49 cells/$D^2$, 22 cells/$D^2$ and 12 cells/$D^2$ (Figure 2(b)) and it is seen that the numerical model calculates the wave forces accurately from 49 cells/$D^2$ onwards. Mo et al. (2007) reported that the measured wave forces corresponded to the force calculated from the inertia part of the Morison equation. So, this case is inertia-dominated with low influence from the viscous boundary layer. The numerical model employs wall layer turbulence modeling and this is

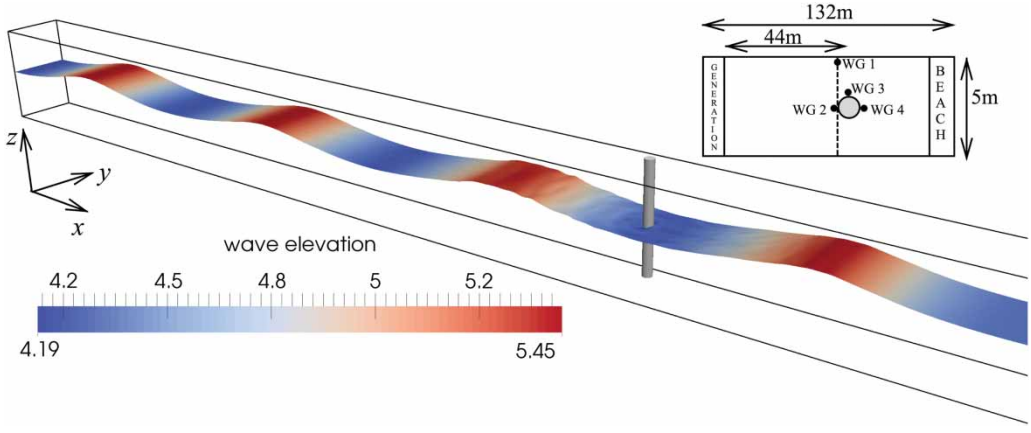


Figure 1. Set-up for calculating forces on a single cylinder.

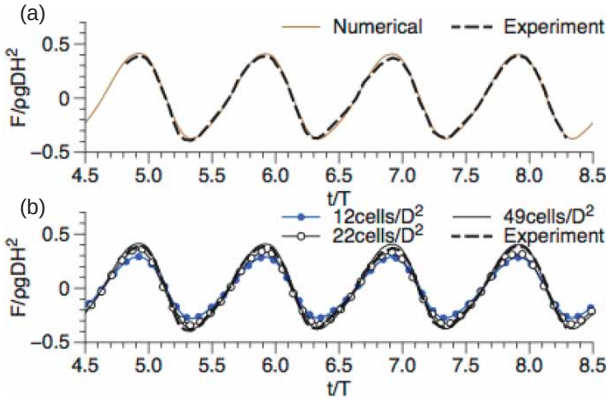


Figure 2. Wave forces on a single cylinder: (a) comparison of experimental and numerical results; (b) grid convergence study for wave forces.

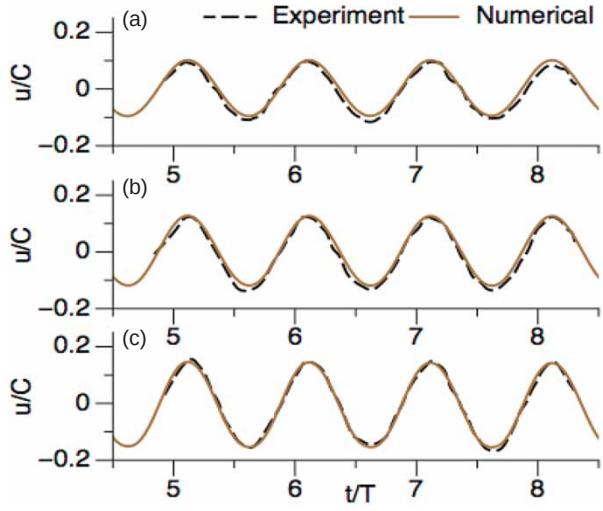


Figure 4. Comparison of experimental and numerical results for water particle velocities in front of the cylinder: (a) at $z = -0.93$ m; (b) at $z = -1.53$ m; (c) at $z = -2.73$ m.

sufficient to account for the hydrodynamics close to the surface of the cylinder in this case. This is also the case for the simulations carried out in the following sections, where the forces are inertia-dominated due to the low KC numbers.

The free surface elevation near the wall along the front line of the cylinder is compared with the experimental data (Figure 3(a)). The amplitude of the wave near the wall along the front line of the cylinder is taken as $\eta_{max,wall}$. The comparisons of the free surface in front, at the side and behind the cylinder are presented in Figure 3(b), 3(c) and 3(d), respectively. The rise in the water level in front of the cylinder recorded in the experiments is seen in the numerical results as well. The water elevations beside and behind the cylinder also show a good match with the experimental observations. Further, the fluid velocity computed by the numerical model is compared with the experimental results. The values are scaled with wave celerity $C$ and are presented in Figure 4; a good agreement is seen between the numerical and experimental results. Thus, it is concluded that the numerical model produces a good representation of the wave elevation, water particle velocity and wave force.

### 4.2. *Wave interaction with multiple cylinders*

#### 4.2.1. *Wave interaction with three cylinders placed in tandem*

Three cylinders of diameter $D = 0.26$ m are placed in tandem with a center-to-center distance $S = 0.8$ m (Figure 5). Linear waves of amplitude $A = 0.03$ m, wavelength $L = 2.0$ m and wave period $T = 1.18$ s ($KC = 0.79$) in a water depth $d = 0.5$ m are generated in a wave tank 15 m long, 5 m wide and 1 m high, with a grid resolution of 108 cells/$D^2$ around each cylinder, resulting in 4.8 million cells. The width of the tank is selected such that reflections from the side wall do not reach the region around the cylinders by ensuring a distance of $9D$ between the wall and the cylinder closest to the wall. The clear distance between the surfaces of the neighboring cylinders in the set-up is $0.27L$ and the wave diffraction and interference effects over a quarter of the incident wavelength are studied. The computed wave forces on the three cylinders are compared with the predictions from the analytical formula (Equation 15)

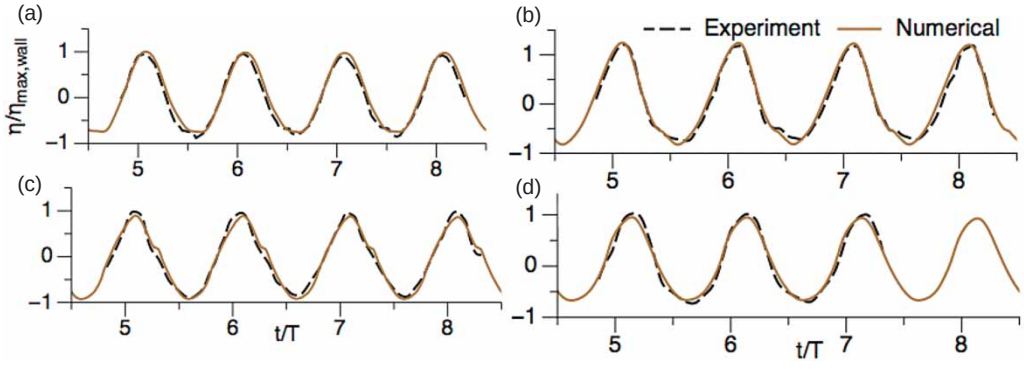


Figure 3. Comparison of experimental and numerical results for wave elevations around the cylinder: (a) at WG 1; (b) at WG 2; (c) at WG 3; d) at WG 4.

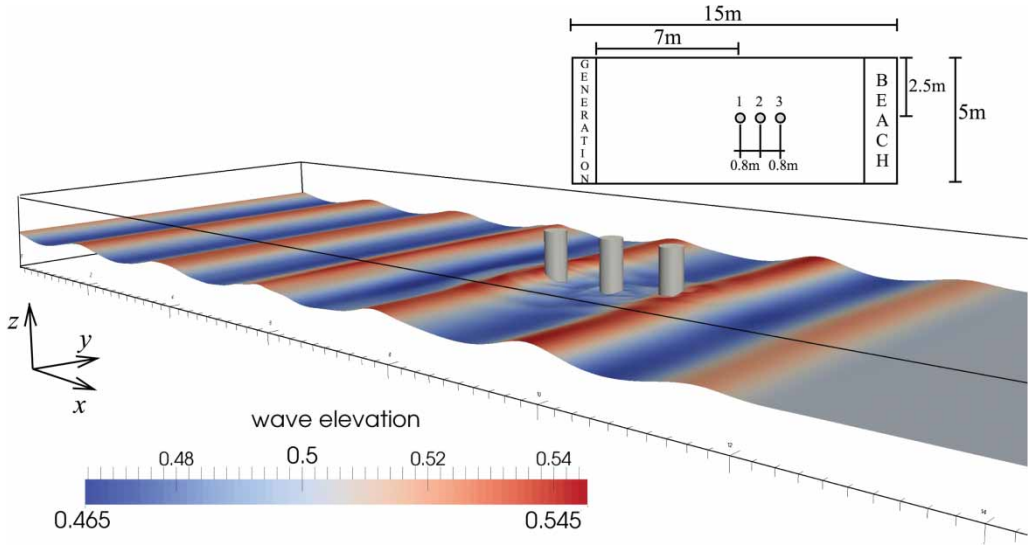


Figure 5. Set-up for three cylinders placed in tandem.

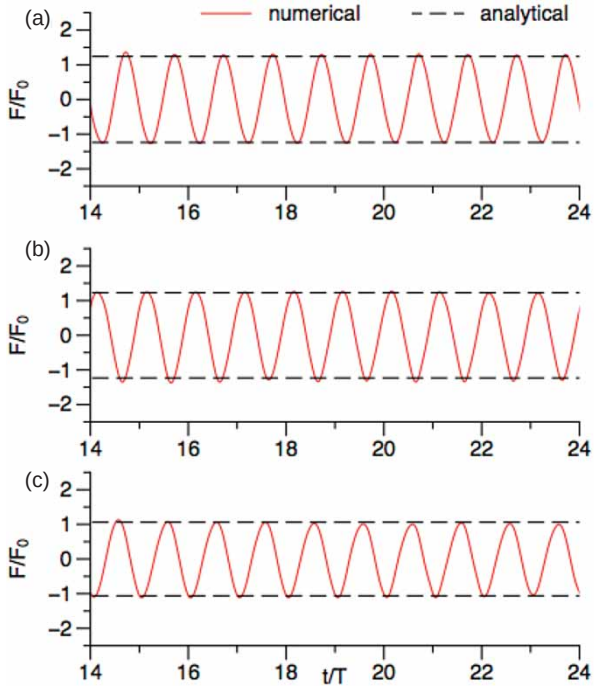


Figure 6. Wave forces on three cylinders placed in tandem: (a) Cylinder 1; (b) Cylinder 2; (c) Cylinder 3.

and a good agreement is seen in Figure 6. Cylinders 1 and 2 experience a similar force of $1.24F_0$ and $1.23F_0$ and the downstream cylinder experiences a force of $1.06F_0$. The interaction of the incident waves and the diffracted waves from the cylinders results in the wave pattern seen in Figure 7 for $t/T = 9.0$, 9.25, 9.50 and 9.75. A circular diffracted wave pattern is noticed in the vicinity of Cylinder 1, which decays as it propagates away from the cylinder. In an inertia-dominated force regime, the pressure around the cylinders influences the forces acting on the cylinders, which can be studied using the free surface elevations. In Figure 7(a), Cylinder 1 is directly exposed to the incident wave crest in the front and a diffracted wave trough is behind the cylinder. This leads to a larger net difference in the pressure around the cylinder, resulting in a higher force compared to a single cylinder. The constructive interference seen in Figure 7(b) results in a larger wave elevation behind Cylinder 1, when a wave trough is incident on it in the front. Thus, Cylinder 1 is always subject to large differences in pressure and it experiences a force that is larger than the force experienced by a single cylinder. Cylinder 2 is exposed to scattered waves from both the upstream Cylinder 1 and the downstream Cylinder 3. This counteracts the shadowing of the incident waves by Cylinder 1, and Cylinder 2 experiences a force higher than the force on a single cylinder. A similar interaction is noted between Cylinders 2 and 3, but Cylinder 3 experiences a lower force of $1.06F_0$ because it is largely exposed only to the scattered waves from upstream Cylinders 1 and 2. It is also clearly seen from Figure 7(c) and 7(d) that the diffracted waves from Cylinder 1 radiate away along the $y$-axis and the diffracted pattern along $x$-axis is extended until the vicinity of Cylinder 3. The diffracted waves from the cylinders upstream interact with each other and the diffracted waves from Cylinder 3, resulting in a slightly higher force than on a single cylinder on Cylinder 3. The total inline wave forces are seen to decrease along the direction of wave propagation. As the wave crest is incident on Cylinder 1, the flow is obstructed and the waves are scattered around the cylinder, resulting in a downstream pressure gradient. A diffracted wave is radiated from Cylinder 1, which propagates further downstream and interacts with the diffracted waves radiated from Cylinder 2. This complex interaction between the cylinders leads to higher forces on both Cylinders 1 and 2 compared to the forces on a single cylinder.

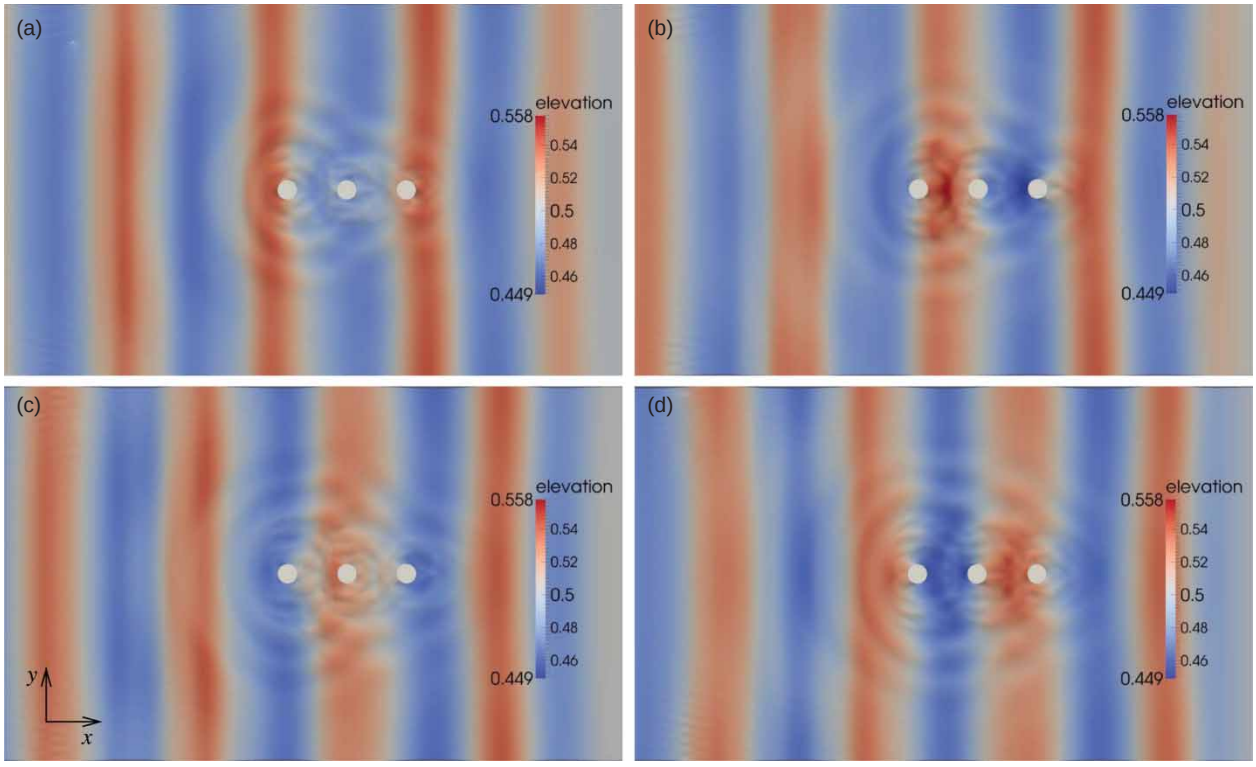


Figure 7. Wave elevations around the cylinders showing wave diffraction patterns: (a) $t/T = 9.0$; (b) $t/T = 9.25$; (c) $t/T = 9.50$; (d) $t/T = 9.75$.

#### 4.2.2. *Wave interaction with three cylinders placed side by side*

In this case, three cylinders of diameter $D = 0.26$ m are placed next to each other with a center-to-center distance of $S = 0.3$ m. A small center-to-center distance is chosen to magnify the effects of flow obstruction caused by the cylinders. Regular linear waves of amplitude $A = 0.03$ m, wavelength $L = 2.0$ m and wave period $T = 1.18$ s ($KC = 0.79$) in a water depth $d = 0.5$ m are generated in a wave tank 15 m long, 7 m wide and 1 m high, with a grid resolution of 108 cells/$D^2$ around each cylinder, resulting in 6.72 million cells.

The cylinders on either side experience the same force of $1.31F_0$, due to the symmetrical arrangement of the cylinders. The central cylinder experiences the maximum force of $1.58F_0$ in the array and the numerical results in Figure 8 show a good match between the computed wave forces and the results from the analytical solution. The contraction effect due to the small distance of separation $S = 0.3$ m between the centers of the cylinders seen in Figure 9 results in a large pressure difference in front and behind the cylinders. This is seen through the increase in the water level in front of the cylinders and lower water elevations behind the cylinders. The distinct increase in water elevation in front of Cylinder 2 during the incidence of the crest and the propagation of the elevated water level through the space around the cylinder is clearly seen in Figure 9. The circular diffracted waves radiating from the

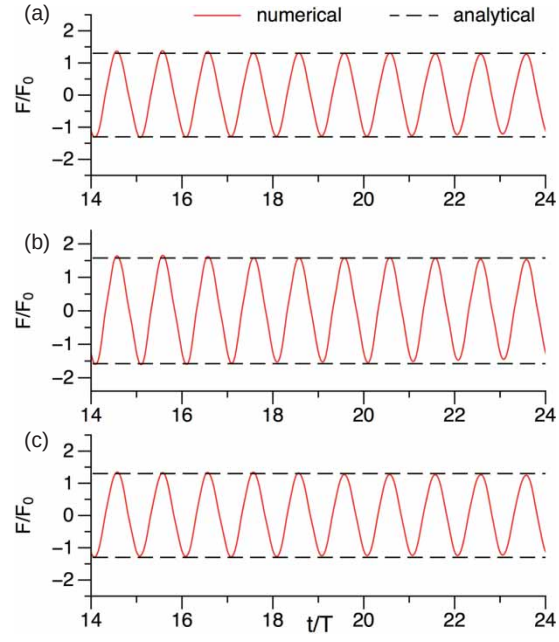


Figure 8. Wave forces on cylinders placed side-by-side: (a) Cylinder 1; (b) Cylinder 2; (c) Cylinder 3.

group of cylinders is also observed. The result of the flow obstruction is a large pressure in front of the cylinders and a much lower pressure behind them. This large difference in the net pressure leads to a 31% larger force on Cylinders 1 and 3 (Figure 9(b) and 9(f)) and 58% larger force on

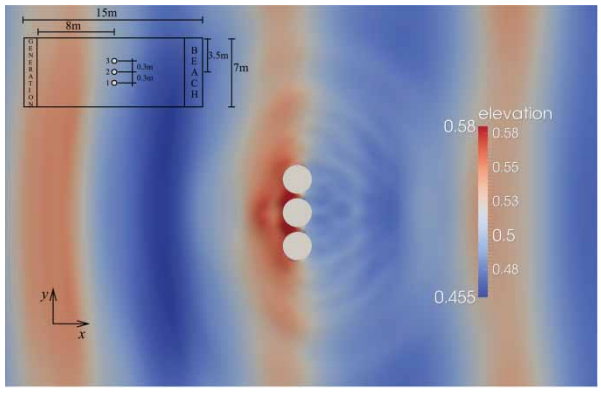


Figure 9. Set-up for three cylinders placed side by side and wave elevation contours around the cylinders.

Cylinder 2 (Figure 9(d)) in comparison to the total force on a single cylinder.

#### 4.2.3. *Wave interaction with a 3 × 3 square array of nine cylinders*

In this case, a 3 × 3 square array of cylinders of diameter $D = 0.26$ m (Figure 10) was placed in a wave tank 16 m long, 7 m wide and 1 m high to study the wave interaction with a large array of cylinders (Figure 11). Waves of amplitude $A = 0.03$ m, wavelength $L = 2.0$ m and wave period $T = 1.18$ s ($KC = 0.79$) in a water depth of $d = 0.5$ m are incident on the cylinder array. The computational domain consists of a grid resolution of 64 cells/$D^2$ around each cylinder with $S = 0.8$ m. Figure 11 shows the wave forces on cylinders and wave surface elevation at $t/T = 11$, 11.25 and 11.5 (Figure 11(a)–11(c)) in the part of the computational domain around the cylinder array. The computed wave forces on the cylinders are in good agreement with the results from the analytical formula. The wave forces on Cylinders 1, 2 and 3 are the same as the wave forces on Cylinders 7, 8 and 9 due to the symmetrical arrangement. Figure 11(a)–11(c) illustrates the interaction of the waves with a 3 × 3 square array of cylinders and the resulting wave patterns due to the incident, diffracted and reflected waves in the computational domain. An increase in the free surface elevation in front of each of the columns of the arrangement is seen in Figure 11(a)–11(c) similar to the increase seen in the case of a single column in section 4.2.2. It is also observed that the increase in the water elevation in front of the cylinders is reduced as the wave progresses downstream. The formation of diffracted waves of large radii is seen behind the first upstream column, showing that the strongest diffracted waves propagate between the first and the second columns in the array. This is similar to the phenomenon observed in section 4.2.1 where the strongest diffracted waves were seen to propagate between the first and second tandem cylinders.

The radiating diffracted waves from cylinders influence the wave forces on the cylinders besides and diagonally across from each cylinder. The central cylinder (Cylinder 4) in the front row experiences the highest force in the array of $1.46F_0$, due to the combined influence of the cylinders beside and behind it (Figure 11(g)). The other two cylinders in the front row (Cylinders 1 and 7) experience a force of $1.34F_0$ (Figure 11(d)). The results are consistent with the case of three cylinders side by side, presented in section 4.2.2, where the central cylinder experienced the maximum force in the column and the two cylinders on either side had lower forces acting on them. Cylinders 2 and 8 in the

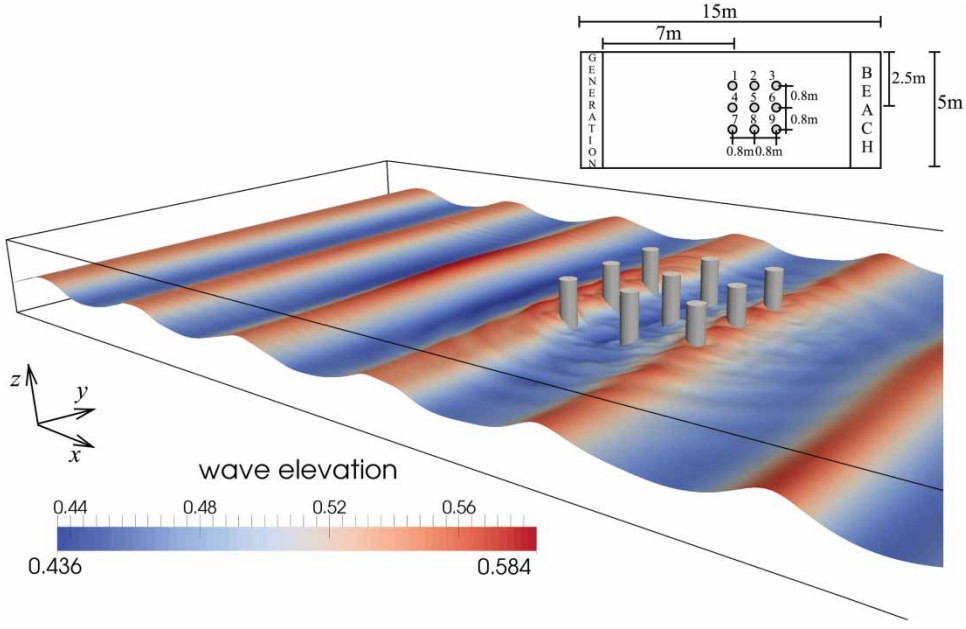


Figure 10. Set-up for nine cylinders placed in a 3 × 3 square array.

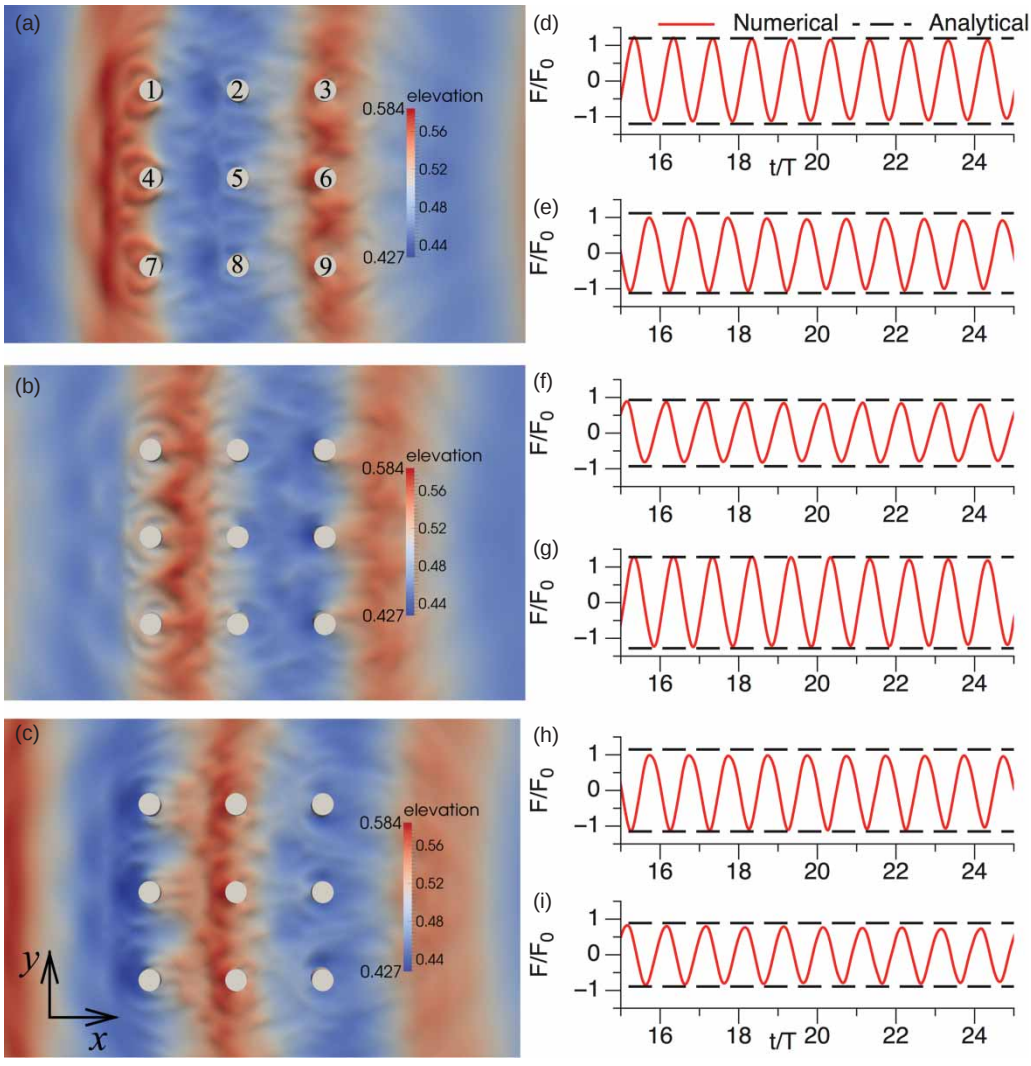


Figure 11. Wave elevations around the cylinders: (a) at $t/T = 11.0$; (b) at $t/T = 11.25$; (c) at $t/T = 11.50$; and wave forces on (d) Cylinder 1; (e) Cylinder 2; (f) Cylinder 3; (g) Cylinder 4; (h) Cylinder 5; (i) Cylinder 6.

second row experience a force of $1.15F_0$ (Figure 11(e)) due to the diffraction effects from the cylinders upstream and downstream. Cylinders 3, 6 and 9 in the downstream row experience the lowest forces in the array as they are protected from the direct incident waves by the upstream cylinders and do not have cylinders placed behind them. The wave forces on the cylinders reduce along the row in the direction of wave propagation, as seen in the case of three tandem cylinders in section 4.2.1. Cylinders 3 and 9 experience a force of $0.92F_0$ (Figure 11(f)) and Cylinder 6 a force of $0.96F_0$ (Figure 11(i)). The central cylinder in the array is exposed to diffracted and reflected waves from upstream and downstream cylinders. The central position of Cylinder 5 results in diffraction effects from all directions and the cylinder experiences a force of $1.26F_0$ (Figure 11(h)).

In order to study the influence of the center-to-center distance between the cylinders, simulations with $S = 0.6$ m and $S = 1.0$ m were carried out with the incident wavelength kept at $L = 2$ m. The numerically determined amplitude of the wave forces on each of the cylinders in the different cases is compared and presented in Figure 12. It is seen that for $S = 0.6$ m, the cylinders in the first column (Cylinders 1, 4 and 7) experience the same force, lower than the force on a single cylinder, $F_0$. The cylinders in the second column (Cylinders 2, 5 and 8) experience the highest forces in the arrangement and the cylinders in the last column (Cylinders 3, 6 and 9) experience forces higher than $F_0$. In this case, a different diffraction regime arises from the center-to-center distance, being much less than half of the incident wavelength compared to $S = 0.8$ m. The cylinders in the second row experience higher forces than the cylinders in the first row because of the destructive interference of the diffracted waves around the first column and constructive interference around the second column in this arrangement.

On the other hand, at $S = 1.0$ m, the cylinders in the first column experience the same force as that on a single

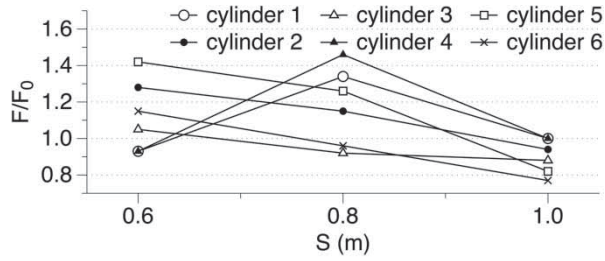


Figure 12. Variation of the wave forces on the cylinders with a distance of separation S.

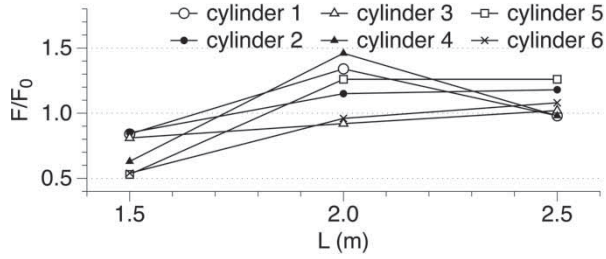


Figure 13. Variation of the wave forces on the cylinders with incident wavelength L.

cylinder, $F_0$. The cylinders in the second and third columns experience forces lower than $F_0$. This is justified by the fact that the cylinders are placed wide apart at $S = 1.0$ m and the wave forces experienced by the cylinders in the first column are the same as those experienced by a single cylinder. As the wave propagates through the array, the interaction with the cylinders reduces the wave energy carried by it and successive columns experience lower forces. The central cylinder (Cylinder 5) benefits from cancelation effects from two sides and experiences a lower force than Cylinder 3 in the third column.

The effect of incident wavelength on the wave forces experienced by the cylinders in the arrangement is studied by carrying out simulations with $L = 1.5$ m and $L = 2.5$ m. The center-to-center distance between the cylinders is kept at $S = 0.8$ m. The variation of the wave forces on the cylinders in the array with the incident wavelength is presented in Figure 13. A general trend of the wave forces increasing with increasing incident wavelength is seen. It is also observed that the change in incident wavelength does not greatly affect the wave forces on Cylinders 3, 6 and 9 in the last column. The central cylinder in the first column, Cylinder 4, undergoes the most change in the wave forces with change in the incident wavelength. The center-to-center distance of $S = 0.8$ m is almost equal to half the incident wavelength for $L = 1.5$ m, but the wave forces on all the cylinders are seen to be lower than the force on a single cylinder. The highest increase in the forces is seen when the incident wavelength is increased from $L = 1.5$ m to $L = 2$ m. This is further evidence that the strong diffraction and interference effects occur between the cylinders when the center-to-center distance is slightly lower than but not equal to half the incident wavelength.

## 5. Conclusion

The open-source CFD model REEF3D was used to model the wave interaction with a single vertical cylinder, three cylinders placed in tandem, three cylinders placed side by side and a $3 \times 3$ square array of nine cylinders at low KC numbers. The numerical model was validated by comparing the numerical results with the experimental data from the large-scale experiments performed by Mo et al. (2007). The computed wave surface elevation, water particle velocity and wave forces on a single cylinder agree well with the experimental data.

The wave interaction with cylinder groups in different configurations was investigated. Circular diffracted waves were observed radiating from the cylinders with constructive and destructive wave interference influencing the wave forces on the cylinders. The following observations were made in each of the cases simulated:

*Three cylinders in a tandem arrangement:*

- The computed wave forces on the first two cylinders were about 24% larger than the wave forces on a single cylinder due to the strong interaction of the diffracted waves between them. The last cylinder in the array experienced only a 6% higher force than a single cylinder due to the absence of neighbors downstream from the cylinder.

*Three cylinders in a side-by-side arrangement:*

- An increase in the free surface elevation in front of the column of cylinders was observed due to the flow obstruction caused by the three closely-spaced cylinders.
- The central cylinder experienced a 57% higher force than a single cylinder and the cylinders beside it experienced a similar force that was 30% higher than the force experienced by a single cylinder.

*Nine cylinders in a $3 \times 3$ square array arrangement:*

- The circular radiating waves from each of the cylinders had an influence on all the cylinders in the arrangement.
- The cylinders experience the highest forces when the center-to-center distance is slightly less than half the incident wavelength due to the constructive wave interference around the cylinders.
- The central cylinder in the first column experiences the largest change in the wave force on changing the incident wavelength.

The paper presents the results for three cylinders arranged in tandem and side by side. Further a combination of these two cases, a 3 × 3 square array of cylinders, was simulated and the effect of incident wavelength and center-to-center distance on the wave forces was investigated. The results obtained in this study represent a few combinations of cylinder arrangements. Further studies can be carried out to explore the influence of the center-to-center distance and the incident wavelength on the wave forces. The variation of the force regime for high steepness waves and larger cylinders can also be investigated.

## Disclosure statement

No potential conflict of interest was reported by the author(s).

## Funding

This work was supported by the OWCBW Project funded by the Research Council of Norway (grant number 217622/E20). This work was supported in part with computational resources provided by the Norwegian University of Science and Technology (NTNU) by NOTUR, http://www.notur.no.

## ORCID

*Arun Kamath* http://orcid.org/0000-0001-8324-9482
*Mayilvahanan Alagan Chella*
http://orcid.org/0000-0002-5462-966X
*Hans Bihs* http://orcid.org/0000-0002-8726-1283

## References

Alagan Chella, M., Bihs, H., Myrhaug, D., & Muskulus, M. (2015). Breaking characteristics and geometric properties of spilling breakers over slopes. *Coastal Engineering*, *95*, 4–19.

Berthelsen, P. A., & Faltinsen, O. M. (2008). A local directional ghost cell approach for incompressible viscous flow problems with irregular boundaries. *Journal of Computational Physics*, *227*, 4354–4397.

Bihs, H. (2011). *Three-dimensional numerical modeling of local scouring in open channel flow* (PhD thesis). Department of Hydraulic and Environmental Engineering, NTNU Trondheim.

Bradshaw, P., Ferriss, D. H., & Atwell, N. P. (1967). Calculation of boundary-layer development using the turbulent energy equation. *Journal of Fluid Mechanics*, *28*, 593–616.

Chau, K. W., & Jiang, Y. W. (2001). 3D numerical model for Pearl river estuary. *Journal of Hydraulic Engineering*, *127*, 72–82.

Chau, K. W., & Jiang, Y. W. (2004). A three-dimensional pollutant transport model in orthogonal curvilinear and sigma coordinate system for Pearl river estuary. *International Journal of Environment and Pollution*, *21*(2), 188–198.

Chorin, A. (1968). Numerical solution of the Navier-Stokes equations. *Mathematics of Computation*, *22*, 745–762.

del Jesus, M., Lara, J. L., & Losada, I. J. (2012). Three-dimensional interaction of waves and porous coastal structures: Part I: Numerical model formulation. *Coastal Engineering*, *64*, 57–72.

Durbin, P. A. (2009). Limiters and wall treatments in applied turbulence modeling. *Fluid Dynamics Research*, *41*, 1–18.

Griebel, M., Dornsheifer, T., & Neunhoeffer, T. (1998). *Numerical simulation in fluid dynamics: A practical introduction*. Philadelphia, PA. Society for Industrial and Applied Mathematics.

Harten, A. (1983). High resolution schemes for hyperbolic conservation laws. *Journal of Computational Physics*, *49*, 357–393.

Higuera, P., Lara, J. L., & Losada, I. J. (2014). Three-dimensional interactions of waves and porous coastal structures using OpenFOAM: Part I: Formulation and validation. *Coastal Engineering*, *83*, 253–258.

Isaacson, M de St Q. (1982). Nonlinear-wave effects on fixed and floating bodies. *Journal of Fluid Mechanics*, *120*, 267–281.

Jacobsen, N. G., Fuhrman, D. R., & Fredsøe, J. (2012). A wave generation toolbox for the open-source CFD library: OpenFOAM. *International Journal for Numerical Methods in Fluids*, *70*, 1073–1088.

Jiang, G. S., & Shu, C. W. (1996). Efficient implementation of weighted ENO schemes. *Journal of Computational Physics*, *126*, 202–228.

Kim, S. K., Liu, P. L-F., & Ligget, J. A. (1983). Boundary integral equation solutions for solitary wave generation, propagation and run-up. *Coastal Engineering*, *7*, 299–317.

Linton, C. M., & Evans, D. V. (1990). The interaction of waves with arrays of vertical circular cylinders. *Journal of Fluid Mechanics*, *215*, 549–569.

Liu, T., & Yang, J. (2014). Three-dimensional computations of water-air flow in a bottom spillway during gate opening. *Engineering Applications of Computational Fluid Mechanics*, *8*(1), 104–115.

Longuet-Higgins, M. S., & Cokelet, E. D. (1976). The deformation of steep surface waves on water I – A numerical method of computation. *Proceedings of the Royal Society of London. Series A, Mathematical and Physical Sciences*, *350*, 1–26.

MacCamy, R., & Fuchs, R. (1954). *Wave forces on piles: A diffraction theory* (Technical Memorandum No. 69). Washington, DC: Beach Erosion Board, Coastal Engineering Research Center, US Army.

Mayer, S., Garapon, A., & Sørensen, L. S. (1998). A fractional step method for unsteady free-surface flow with applications to non-linear wave dynamics. *International Journal for Numerical Methods in Fluids*, *28*(2), 293–315.

Mo, W., Irschik, K., Oumeraci, H., & Liu, P. (2007). A 3D numerical model for computing non-breaking wave forces on slender piles. *Journal of Engineering Mathematics*, *58*, 19–30.

Morgan, G. C. J., Zang, J., Greaves, D., Heath, A., Whtilow, C. D., & Young, J. R. (2010). Using the rasInterFoam CFD model for wave transformation and coastal modeling. *Proceedings of the Coastal Engineering Conference*, Shanghai, China, 1–9.

Morison, J. R., O'Brien, M. P., Johnson, J. W., & Schaaf, S. A. (1950). Force exerted by surface waves on piles. *Journal of Petroleum Technology*, *2*, 149–154.

Naot, D., & Rodi, W. (1982). Calculation of secondary currents in channel flow. *Journal of the Hydraulic Division. Proceedings of the American Society of Civil Engineers*, *108*(HY 8), 948–968.

Nwogu, O. (1993). Alternative form of Boussinesq equations for nearshore wave propagation. *Journal of Waterway, Port, Coastal, and Ocean Engineering*, *119*(6), 618–638.

Ohkusu, M. (1974). Hydrodynamic forces on multiple cylinders in waves. *Proceedings of the International Symposium on Dynamics of Marine Vehicles and Structures in Waves.* London, 107–112.

Osher, S., & Sethian, J. A. (1988). Fronts propagating with curvature-dependent speed: algorithms based on Hamilton-Jacobi formulations. *Journal of computational physics*, *79*(1), 12–49.

Peng, D., Merriman, B., Osher, S., Zhao, H., & Kang, M. (1999). A PDE-based fast local level set method. *Journal of Computational Physics*, *155*, 410–438.

Peskin, C. S. (1972). Flow patterns around the heart valves: A numerical method. *Journal of Computational Physics*, *10*, 252–271.

Pu, J. H., Shao, S., Huang, Y., & Hussain, K. (2013). Evaluations of SWEs and SPH numerical modelling techniques for dam break flows. *Engineering Applications of Computational Fluid Mechanics*, *7*(4), 544–563.

Spring, B., & Monkmeyer, P. L. (1974). Interaction of plane waves with vertical cylinders. *Proceedings of the International Conference on Coastal Engineering, ASCE*, Copenhagen, 1828–1847.

Sussman, M., Smereka, P., & Osher, S. (1994). A level set approach for computing solutions to incompressible two-phase flow. *Journal of Computational physics*, *114*(1), 146–159.

van der Vorst, H. (1992). Bi-CGStab: A fast and smoothly converging variant of Bi-CG for the solution of non symmetric linear systems. *SIAM Journal on Scientific and Statistical Computing*, *13*, 631–644.

Wei, G., & Kirby, J. T. (1995). Time-dependent numerical code for extended Boussinesq equations. *Journal of Waterway, Port, Coastal and Ocean Engineering*, *121*(5), 251–261.

Wilcox, D. C. (1994). *Turbulence modeling for CFD*. La Canada, California: DCW Industries Inc.